Superpixel construction for hyperspectral unmixing

Zeng Li[(1,2)], Jie Chen[(2,1)], Susanto Rahardja[(1)]
[(1)]Centre of Intelligent Acoustics and Immersive Communications
School of Marine Science and Technology, Northwestern Polytechinical University, Xi'an, China
[(2)]Research & Development Institute of Northwestern Polytechnical University, Shenzhen, China
lizeng@mail.nwpu.edu.cn {dr.jie.chen, susantorahardja}@ieee.org

***Abstract*—Spectral unmixing aims to determine the component materials and their associated abundances from mixed pixels in a hyperspectral image. Instead of performing unmixing independently on each pixel, investigating spatial and spectral correlations among pixels can be beneficial to enhance the unmixing performance. However linking pixels across an entire image for such a purpose can be computationally cumbersome and physically unreasonable. In order to address this issue, we propose to construct superpixels for hyperspectral data unmixing. Using an SLIC-based (Simple Linear Iterative Clustering) superpixel constructing process, adjacent pixels are clustered into several blocks with similar spectral signatures. After this preprocessing, unmixing is then performed with a graph-based total variation regularization to benefit from the heterogeneity within each superpixel. Experimental results on synthetic data and real hyperspectral data illustrate advantages of the proposed scheme.**

***Index Terms*—Hyperspectral images, spectral unmixing, superpixel analysis, graph regularization**

I. Introduction

Due to the limitation of spatial resolution and intimate interactions of materials, the observed reflectance at each pixel of hyperspectral data is typically a mixture of several spectral signatures of several pure materials. Spectral unmixing is thus an important task for hyperspectral data processing to analyze information in each pixel. It usually consists of extracting the spectral signatures and evaluating their associated fraction abundances [1], [2].

Instead of performing the spectral unmixing on each individual pixel, it can be beneficial to investigate spectral or spatial correlation among pixels to enhance the estimation performance. For instance, in [3] authors present the spatial-spectral coherence regularization that was imposed to allow abundance estimation for a pixel to be influenced by its spectrally similar and spatially adjacent neighbors. In [4], [5] authors propose to include the total variation regularization into the unmixing to achieve the piecewise spatial consistency of estimated abundances. In [6], a nonlocal total variance regularization is imposed on the reconstructed spectra rather than directly on the abundances over the entire image and in [7], a graph Laplacian regularization (GLUP-Lap) is introduced over the entire image, and the spectral clustering, computational intensive for a large image, is applied to the constructed graph.

The work of Jie Chen was supported in part by Natural Science Foundation of Shenzhen under grant JCYJ2017030155315873.

In [8], authors perform the unmixing with low-rank spatial regularization within fixed-size square windows. However, in [4]–[7] linking pixels across an entire image, either in the sense of spatial correlation or spectral correlation, can be computationally cumbersome and physically unreasonable. Further, like in [8] using regularization in fixed square windows can be sub-optimal since the form of such a window is not coherent with image textures. In order to address this issue, we propose to construct superpixels for hyperspectral data unmixing.

Recently superpixels analysis has been used for hyperspectral applications, such as dimensionality reduction [9], hyperspectral change detection [10], classification [11], hyperspectral images segmentation [12] and spectral unmixing [13], [14]. In [13], authors use AVMAX and MVES, two typical endmember extraction algorithms for endmember extraction on the superpixel set. In [14], authors use a modified SLIC algorithm of [15] for endmember extraction, followed by further fine tuning steps to obtain final endmembers. These works use superpixels to benefit endmember extraction, however abundance estimation is performed with common methods.

In this paper, we concentrate on using superpixels to improve the fractional abundance estimation. In order to make use of the spatial-spectral information better,we construct superpixels for a hyperspectral image via an SLIC-based algorithm, and perform the spectral unmixing using a graph regularization within each superpixel. Since the number of superpixels is significantly smaller than the number of pixels in the original image, unmixing within each superpixel largely reduces computational burden. Further, compared to spatial regularization within windows of a fixed size, unmixing performance can also be enhanced thanks to the spectral homogeneity within superpixels. Then Alternating Direction Method of Multipliers (ADMM) is used for solving the unmixing problems. The Simulations with both synthetic and real data validate the proposed scheme.

II. Data model

Notation. Normal font x or X denotes scalars. Boldface small letters $\mathbf{x}$ and capital letters $\mathbf{X}$ denote column vectors and matrices, respectively. The superscript $(\cdot)^\top$ denotes the transpose operator. $\|\mathbf{X}\|_{\mathrm{F}}$ and $\|\mathbf{X}\|_{1,1}$ denote the Frobenius norm and the $\ell_{1,1}$ norm of the matrix argument $\mathbf{X}$ respectively. $\|\mathbf{x}\|_1$ denotes the ℓ_1 norm of vector $\mathbf{x}$.

ISBN 978-90-827970-1-5

Suppose that the hyperspectral image under study has w pixels in each row and h pixels in each column. Each pixel consists of a reflectance vector in L contiguous spectral bands. In order to facilitate the presentation, we transform this 3-D data into an $L \times N$ matrix, with $N = w \times h$ being the total number of pixels. Then, let $\mathbf{R} = [\mathbf{r}_1, \ldots, \mathbf{r}_N] \in \mathbb{R}^{L \times N}$ be the observed reflectance vectors, consisting of a mixture of at most R signature spectra, $\mathbf{S} = [\mathbf{s}_1, \ldots, \mathbf{s}_R] \in \mathbb{R}^{L \times R}$ be the endmember matrix, which is a spectral library consisting of spectral signatures $\mathbf{s}_i$, and $\mathbf{X} = [\mathbf{x}_1, \ldots, \mathbf{x}_N]$ be the matrix composed of all the abundance vectors. In the scope of this work, we consider the linear mixture model where an observed pixel is a combination of signature spectra weighted by the abundances, namely,

$$\mathbf{R} = \mathbf{S}\mathbf{X} + \mathbf{Z} \tag{1}$$

where $\mathbf{Z} \in \mathbb{R}^{L \times N}$ is the modeling noise. To be physically meaningful, it is often required that each column of $\mathbf{X}$ is subject to two constraints, abundance nonnegative constraint (ANC) and abundance sum-to-one constraint (ASC).

III. Superpixel construction for hyperspectral data

In this section, we propose a strategy to construct superpixels for a hyperspectral image. Considering the simplicity and effectiveness of the conventional SLIC algorithm, an SLIC-based algorithm is proposed to construct superpixels in the context of hypsepctral image analysis.

The algorithm SLIC can be viewed as a specific form of k-means clustering and has been widely used in image segmentation. In brief, for color images in the CIELAB space, the algorithm clusters pixels with a multiple dimensional feature composed by color channels and pixel coordinates to efficiently generate compact, nearly uniform superpixels. It is straightforward to extend SLIC to hyperspectral data. Let $D(i,j)$ denote the dissimilarity between two pixels i and j, and it is calculated by combining the spatial distance $d_s(i,j)$ and spectral distance $d_c(i,j)$ via:

$$D(i,j) = \sqrt{d_c^2(i,j) + \left[\frac{d_s(i,j)}{S}\right]^2 m^2} \tag{2}$$

$$d_s(i,j) = \sqrt{(x_i - x_j)^2 + (y_i - y_j)^2} \tag{3}$$

$$d_c(i,j) = \|\mathbf{T}(\mathbf{r}_i - \mathbf{r}_j)\| \tag{4}$$

where (x_i, y_i) are coordinates of pixel i, S is the nominal size of a superpixel set by $\sqrt{\frac{N}{k}}$ with k controlling the number of superpixels, and m weighs the relative importance between spectral and spatial similarity. Specifically, matrix $\mathbf{T} \in \mathbb{R}^{L' \times L}$ with $L' < L$ is a transformation matrix to remove spectral redundancies. It can be set to perform band selection or dimension reduction via, for instance, the Principal Component Analysis.

The rationale of using superpixels can be summarized into the following two aspects:

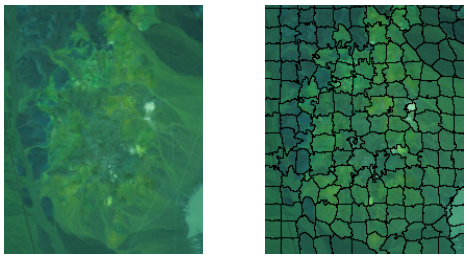

Fig. 1. Left: False color image of Cuprite data. Right: Constructed superpixels with $m = 1.4$ and $k = 180$.

1) Since the sizes of superpixels are significantly smaller than the original image, unmixing within each superpixel will largely reduce computational burden of the analysis.
2) A superpixel is an irregular area of local pixels with homogenous spectra. Irregularity in shape makes the area fit the local image texture, and maximumly contributes to cooperative processing across pixels. Homogeneity of spectra is also beneficial for spatial regularization and sparse estimation.

Fig. 1 shows the superpixel construction result of the AVIRIS Cuprite data by the SLIC-based algorithm. We can see the algorithm partitions this hyperspectral image as expected into local blocks with similar spectra within each block.

IV. Graph-regularized sparse unmixing

In this section, we propose to perform a graph regularized sparse unmixing with the constructed superpixels. In ith superpixel, the unmixing will be performed on $\mathbf{R}^{(i)}$ and $\mathbf{X}^{(i)}$, which respectively denote the pixels and associated abundances in the current superpixel. Other variables that are associated to the i pixels are indicated with superscript $^{(i)}$.

A. Graph Representation

In hyperspectral images, each pixel can be viewed as a node and weights in edges measure the similarity of nodes. The adjacency matrix $\mathbf{A}$ is often used to express a graph whose elements indicate the connectivity of the pairs of nodes. One simple way to construct a graph is considering a four-neighborhood graph in spatial coordinates. In term of spectral dimension, we can measure the spectral similarity (Euclidean distance or spectral angle) among the pixels. In [7], the adjacency matrix $\mathbf{A}$ is defined according to

$$\begin{cases} \mathbf{A}_{k\ell} = 1 & \text{if } \|\mathbf{r}_k - \mathbf{r}_\ell\|_2^2 < \delta, \\ \mathbf{A}_{k\ell} = 0 & \text{otherwise} \end{cases} \tag{5}$$

where δ represents the maximum squared spectral distance required in order to consider that two pixels are similar. Moreover, we can build the spatial-spectral combined graph and some other graph construction techniques, as in [16]. Since working on a graph associated with the entire image can be quite computational intensive, in this work, we construct subgraphs within superpixels that can be considered as a first layer segmentation.

ISBN 978-90-827970-1-5

B. Graph-regularized Linear Unmixing

Based on the linear mixing model (1), the unmixing problem can be expressed in a matrix form under ANC by

$$\min_{\mathbf{X}^{(i)}} \frac{1}{2}\|\mathbf{R}^{(i)} - \mathbf{S}\mathbf{X}^{(i)}\|_F^2 + \mu\|\mathbf{X}^{(i)}\|_{1,1} + \lambda g(\mathbf{X}^{(i)}),$$
$$\text{subject to : } \mathbf{X}^{(i)} \geq 0 \tag{6}$$

where μ and λ are regularization parameters, $\ell_{1,1}$-norm is applied to a superpixel $\mathbf{X}^{(i)}$ for a sparse selection of contributing endmembers from spectral library $\mathbf{S}$, and function g regularizes the estimation via the constructed graph within superpixel i by

$$g(\mathbf{X}^{(i)}) = \sum_{k=1}^{n}\sum_{\ell=1}^{n}[\mathbf{A}^{(i)}]_{k\ell}\|\mathbf{x}_k^{(i)} - \mathbf{x}_\ell^{(i)}\|_1 \tag{7}$$

This term serves as a regularization that penalizes the discrepancies between all pair of estimated abundances weighted via a graph-based total variation. In order to efficiently solve the problem (6), the graph regularized term (7) can equivalently be written using the incidence matrix $\mathbf{B}^{(i)}$ of a graph, that is:

$$\sum_{k=1}^{n}\sum_{\ell=1}^{n}[\mathbf{A}^{(i)}]_{k\ell}\|\mathbf{x}_k^{(i)} - \mathbf{x}_\ell^{(i)}\|_1 = \|\mathbf{X}^{(i)}\mathbf{B}^{(i)}\|_{1,1} \tag{8}$$

Problem (6) can then be written as:

$$\min_{\mathbf{X}^{(i)}} \frac{1}{2}\|\mathbf{R}^{(i)} - \mathbf{S}\mathbf{X}^{(i)}\|_F^2 + \mu\|\mathbf{X}^{(i)}\|_{1,1} + \lambda\|\mathbf{X}^{(i)}\mathbf{B}^{(i)}\|_{1,1}$$
$$\text{subject to : } \mathbf{X}^{(i)} \geq 0 \tag{9}$$

C. Solution via ADMM

We shall now propose to solve the optimization problem (9) via the ADMM algorithm. In order to simplify the notation, we discard the superscript$^{(i)}$ without ambiguity. Introducing auxiliary variables $\mathbf{V}_1$ to $\mathbf{V}_4$, problem (9) can be rewritten as follows:

$$\min_{\mathbf{X}} \frac{1}{2}\|\mathbf{R} - \mathbf{V}_1\|_F^2 + \mu\|\mathbf{V}_2\|_{1,1} + \lambda\|\mathbf{V}_4\|_{1,1} + l_{\mathbb{R}_+^{R\times n}}(\mathbf{V}_2),$$
$$\text{subject to : } \mathbf{V}_1 = \mathbf{S}\mathbf{X}, \mathbf{V}_2 = \mathbf{X}, \mathbf{V}_3 = \mathbf{X}, \mathbf{V}_4 = \mathbf{V}_3\mathbf{B} \tag{10}$$

where $l_{\mathbb{R}_+}(\mathbf{X}) = \sum_{i=1}^{n} l_{\mathbb{R}_+}(\mathbf{x}_i)$ is the indicator function such that $l_{\mathbb{R}_+}(\mathbf{x}_i)$ is 0 if $\mathbf{x}_i$ belongs to the nonnegative orthant and $+\infty$ otherwise. The corresponding augmented Lagrangian is given by:

$$\begin{aligned}
&\mathcal{L}(\mathbf{X}, \{\mathbf{V}_i\}_{i=1}^4, \{\mathbf{D}_i\}_{i=1}^4)\\
=&\frac{1}{2}\|\mathbf{R} - \mathbf{V}_1\|_F^2 + \mu\|\mathbf{V}_2\|_{1,1} + \lambda\|\mathbf{V}_4\|_{1,1} + l_{\mathbb{R}_+^{R\times n}}(\mathbf{V}_2)\\
&+ \frac{\rho}{2}\|\mathbf{S}\mathbf{X} - \mathbf{V}_1 - \mathbf{D}_1\|_F^2 + \frac{\rho}{2}\|\mathbf{X} - \mathbf{V}_2 - \mathbf{D}_2\|_F^2\\
&+ \frac{\rho}{2}\|\mathbf{X} - \mathbf{V}_3 - \mathbf{D}_3\|_F^2 + \frac{\rho}{2}\|\mathbf{V}_3\mathbf{B} - \mathbf{V}_4 - \mathbf{D}_4\|_F^2
\end{aligned} \tag{11}$$

where $\mathbf{D}_1$, $\mathbf{D}_2$, $\mathbf{D}_3$, $\mathbf{D}_4$ are Lagrange multipliers and ρ is the penalty parameter. The solution to (10) can then be achieved by iteratively minimizing $\mathbf{X}$ and $\{\mathbf{V}_i\}_{i=1}^4$, and updating $\{\mathbf{D}_i\}_{i=1}^4$ via the routine of ADMM. The complete algorithm is summarized in Algorithm 1 where soft$(\cdot)$ denotes the row-shrinkage thresholding operator [17].

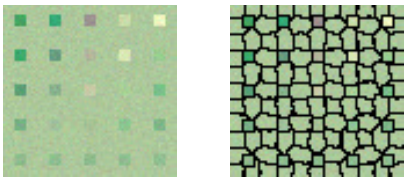

Fig. 2. Left: False color image of Data1. Right: Constructed superpixels of Data1 with $m = 1$ and $k = 120$.

Algorithm 1 Algorithmic path for problem (11)

Input: $\mathbf{S}$, $\mathbf{Y}$, μ, λ, ρ
Output: The estimated abundance $\mathbf{X}$

Initialize: $\mathbf{X}$, $\mathbf{V}_1 \dots \mathbf{V}_4$, $\mathbf{D}_1 \dots \mathbf{D}_4$, $k = 0$
while not converged **do**
  $\mathbf{X}^{k+1} \leftarrow (\mathbf{S}^T\mathbf{S} + 2\mathbf{I})^{-1}[\mathbf{S}^\top(\mathbf{V}_1^k + \mathbf{D}_1^k) + \mathbf{V}_2^k + \mathbf{D}_2^k + \mathbf{V}_3^k + \mathbf{D}_3^k]$
  $\mathbf{V}_1^{k+1} \leftarrow [\rho(\mathbf{S}\mathbf{X}^{k+1} - \mathbf{D}_1^k) + \mathbf{R}](1+\rho)^{-1}$
  $\mathbf{V}_2^{k+1} \leftarrow \max[0, \text{soft}(\mathbf{X}^{k+1} - \mathbf{D}_2^k, \frac{\mu}{\rho})]$
  $\mathbf{V}_3^{k+1} \leftarrow [(\mathbf{V}_4^k + \mathbf{D}_4^k)\mathbf{B}^\top + \mathbf{X}^{k+1} - \mathbf{D}_3^k](\mathbf{I} + \mathbf{B}\mathbf{B}^\top)^{-1}$
  $\mathbf{V}_4^{k+1} \leftarrow \text{soft}(\mathbf{V}_3^{k+1}\mathbf{B} - \mathbf{D}_4^k, \frac{\lambda}{\rho})$
  $\mathbf{D}_1^{k+1} \leftarrow \mathbf{D}_1^k - \mathbf{S}\mathbf{X}^{k+1} + \mathbf{V}_1^{k+1}$
  $\mathbf{D}_2^{k+1} \leftarrow \mathbf{D}_2^k - \mathbf{X}^{k+1} + \mathbf{V}_2^{k+1}$
  $\mathbf{D}_3^{k+1} \leftarrow \mathbf{D}_3^k - \mathbf{X}^{k+1} + \mathbf{V}_3^{k+1}$
  $\mathbf{D}_4^{k+1} \leftarrow \mathbf{D}_4^k - \mathbf{V}_3^{k+1}\mathbf{B} + \mathbf{V}_4^{k+1}$
  Update $k : k = k + 1$
end while

V. Experimental results

In this section, we illustrate the processing results using the proposed scheme via a synthetic hyperspectral data set (denoted by Data1) and a real hyperspectral data set (denoted by Data2).

The first data set Data1 was generated using 5 endmembers containing 75×75 pixels. The endmembers were randomly selected from the USGS spectral library. Each signature of this library has reflectance values measured over 224 spectral bands. The pure regions and mixed regions involved between 2 and 5 endmembers, spatially distributed in the form of square regions. See image DC1 in [4] for details. False color image of Data1 and the constructed superpixels under SNR = 30dB are illustrated in Fig. 2. It is clear that structural patterns in this image are well extracted. We perform the proposed unmixing algorithm along with the constructed superpixels, and compare the results with FCLS [18], SUnSAL-TV and GLUP-Lap in different SNR conditions. The root mean square error (RMSE) is used to evaluate the performance. We test different sparse and spatial regularized parameters μ and λ for SUnSAL-TV, GLUP-Lap and the proposed algorithm. For GLUP-Lap and the proposed algorithm, augmented Lagrange parameter is set to $\rho = 0.5$. Table I shows the performance with optimal parameters set for each algorithm. The proposed scheme results in almost the same RMSE compared to GLUP-Lap, but lower than those of FCLS and SUnSAL-TV. However, it should be noted that the GLUP-lap algorithm involves the

ISBN 978-90-827970-1-5 © EURASIP 2018

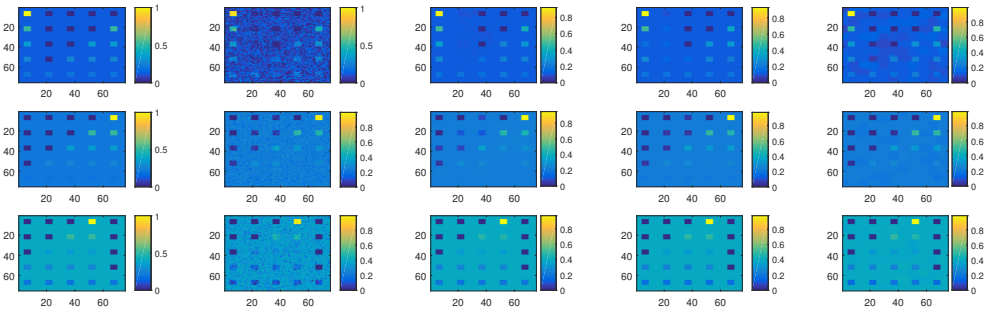

Fig. 3. Estimated abundance maps for Data1. From top to bottom: 1st, 4th, 5th abundance maps. From left to right: True abundance maps, FCLS, SUnSAL-TV, GLUP-Lap and proposed algorithm results.

spectral clustering, where the number of clusters are hard to determine and computational complexity is therefore high due to the eigendecomposition. Table II shows that the processing time of the proposed scheme is much less than that of GLUP-Lap. Fig. 3 illustrates the estimated abundance maps of 1st, 4th and 5th endmembers. Particularly, we observe that in the 1st abundance map the second column of the square regions is better conserved by the proposed scheme.

TABLE I
RMSE EVALUATING PERFORMANCES WITH DIFFERENT VALUES OF SNR IN DATA1, WITH OPTIMAL REGULARIZED PARAMETERS (μ, λ) FOR SUNSAL-TV, GLUP-LAP AND PROPOSED ALGORITHM, THRESHOLDS δ FOR GLUP-LAP AND THE PROPOSED ALGORITHM.

SNR	15dB	20dB	30dB
FCLS	0.0318	0.0262	0.0173
SUnSAL-TV	0.0181 (0.05,0.1)	0.0156 (0.05,0.05)	0.0073 (0.005,0.01)
GLUP-Lap	0.0161 (0.005,1) $\delta = 9$	0.0141 (0.01,0.5) $\delta = 2.5$	0.0049 (5×10^{-4},0.5) $\delta = 0.3$
Proposed	0.0162 (0.3,0.05) $\delta = 9$	0.0141 (0.08,0.05) $\delta = 2.5$	0.0050 (0.05,0.1) $\delta = 0.25$

TABLE II
RUNTIME OF GLUP-LAP AND THE PROPOSED ALGORITHM.

	Data1	Data2
GLUP-Lap	311s	808s
Proposed	77.8s	151s

We also tested algorithms with a real hyperspectral image. The image is captured on the Cuprite mining district by AVIRIS. A sub-image of 250×191 pixels was chosen and it contains 188 spectral bands. The number of endmembers was estimated and set to 12 [19]. VCA algorithm was then used to extract the endmembers. The reconstruction error (RE) (RE $= \sqrt{\frac{1}{NL}\sum_{i=1}^{N} \|\mathbf{y}_i - \hat{\mathbf{y}}_i\|_2^2}$) was used to evaluate performances of algorithms. As shown in Table III, the proposed scheme exhibits a low RE, though it is noted that RE is not always directly related to abundance estimation accuracy. Superpixel

TABLE III
RES OF THE FOUR COMPARED ALGORITHMS WITH OPTIMAL REGULARIZED PARAMETERS (μ, λ) FOR SUNSAL-TV, GLUP-LAP AND PROPOSED ALGORITHM, THRESHOLDS δ FOR GLUP-LAP AND THE PROPOSED ALGORITHM.

	FCLS	SUnSAL-TV	GLUP-Lap	Proposed
RE	0.0068	0.0050 (0.001,0.001)	0.0068 (0.001,1 $\times$ 10^{-4}) $\delta = 0.3$	0.0051 (0.01,1 $\times$ 10^{-4}) $\delta = 0.1$

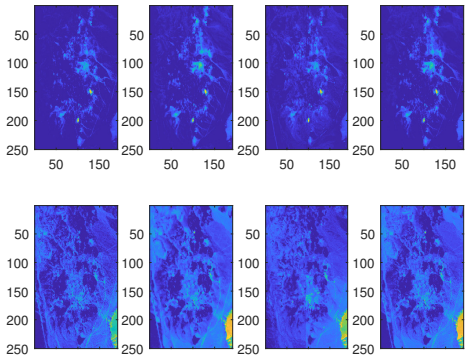

Fig. 4. Abundances maps of selected materials in Data2. From top to bottom: 1st and 8th abundance map. From left to right: FCLS, SUnSAL-TV, GLUP-Lap and proposed algorithm.

analysis result is shown in Fig. 1. Fig. 4 shows 1st and 8th abundance maps where the proposed algorithm highlights localized targets without over smoothing the abundance maps.

VI. CONCLUSION

Hyerpspectral unmixing can benefit from the superpixel construction in abundance estimation performance and computational efficiency simultaneously. In this work we proposed to construct superpixels via an SLIC-based algorithm and perform the unmixing via the graph-regularization. The experimental results confirm the advantages of the proposed scheme. In the future, we will investigate multilayer superpixel construction methods and regularization across superpixels to further increase the flexibility of the proposed scheme.

ISBN 978-90-827970-1-5 © EURASIP 2018

REFERENCES

[1] N. Keshava and J. F. Mustard, "Spectral unmixing," *IEEE Signal Processing Magazine*, vol. 19, no. 1, pp. 44–57, 2002.

[2] J. M. Bioucas-Dias, A. Plaza, N. Dobigeon, M. Parente, Q. Du, P. Gader, and J. Chanussot, "Hyperspectral unmixing overview: Geometrical, statistical, and sparse regression-based approaches," *IEEE Journal of Selected Topics in Applied Earth Observations and Remote Sensing*, vol. 5, no. 2, pp. 354–379, 2012.

[3] A. Castrodad, Z. Xing, J. B. Greer, E. Bosch, L. Carin, and G. Sapiro, "Learning discriminative sparse representations for modeling, source separation, and mapping of hyperspectral imagery," *IEEE Transactions on Geoscience and Remote Sensing*, vol. 49, no. 11, pp. 4263–4281, 2011.

[4] M.-D. Iordache, J. M. Bioucas-Dias, and A. Plaza, "Total variation spatial regularization for sparse hyperspectral unmixing," *IEEE Transactions on Geoscience and Remote Sensing*, vol. 50, no. 11, pp. 4484–4502, 2012.

[5] J. Chen, C. Richard, and P. Honeine, "Nonlinear estimation of material abundances in hyperspectral images with ℓ_1-norm spatial regularization," *IEEE Trans. Geosci. Remote Sens.*, vol. 52, no. 5, pp. 2654–2665, May 2014.

[6] R. Ammanouil, A. Ferrari, and C. Richard, "Hyperspectral data unmixing with graph-based regularization," in *Proc. IEEE GRSS Workshop Hyperspectral Image Signal Processing: Evolution in Remote Sensing (WHISPERS)*, 2015, pp. 1–4.

[7] R. Ammanouil, A. Ferrari, and C. Richard, "A graph laplacian regularization for hyperspectral data unmixing," in *Proc. of the International Conference on Acoustics, Speech and Signal Processing (ICASSP)*, 2015, pp. 1637–1641.

[8] Q. Qu, N. M. Nasrabadi, and T. D. Tran, "Abundance estimation for bilinear mixture models via joint sparse and low-rank representation," *IEEE Transactions on Geoscience and Remote Sensing*, vol. 52, no. 7, pp. 4404–4423, 2014.

[9] X. Zhang, S. E. Chew, Z. Xu, and N. D. Cahill, "Slic superpixels for efficient graph-based dimensionality reduction of hyperspectral imagery," in *Proc. SPIE*, 2015, vol. 9472, p. 947209.

[10] A. Ertürk, S. Ertürk, and A. Plaza, "Unmixing with slic superpixels for hyperspectral change detection," in *Geoscience and Remote Sensing Symposium (IGARSS), 2016 IEEE International*, 2016, pp. 3370–3373.

[11] L. Fang, S. Li, X. Kang, and J. A. Benediktsson, "Spectral–spatial classification of hyperspectral images with a superpixel-based discriminative sparse model," *IEEE Transactions on Geoscience and Remote Sensing*, vol. 53, no. 8, pp. 4186–4201, 2015.

[12] H. Sun and A. Zare, "Map-guided hyperspectral image superpixel segmentation using proportion maps," in *Proc. IEEE Geoscience and Remote Sensing Symposium (IGARSS)*, 2017, pp. 3751–3754.

[13] X. Sun, F. Zhang, L. Yang, B. Zhang, and L. Gao, "A hyperspectral image spectral unmixing method integrating SLIC superpixel segmentation," in *Proc. IEEE GRSS Workshop Hyperspectral Image Signal Processing: Evolution in Remote Sensing (WHISPERS)*. IEEE, 2016, pp. 1–4.

[14] X. Xu, J. Li, C. Wu, and A. Plaza, "Regional clustering-based spatial preprocessing for hyperspectral unmixing," *Remote Sensing of Environment*, vol. 204, pp. 333–346, 2018.

[15] R. Achanta, A. Shaji, K. Smith, A. Lucchi, P. Fua, and S. Süsstrunk, "Slic superpixels compared to state-of-the-art superpixel methods," *IEEE Transactions on Pattern Analysis and Machine Intelligence*, vol. 34, no. 11, pp. 2274–2282, 2012.

[16] J. R. Stevens, R. G. Resmini, and D. W. Messinger, "Spectral-density-based graph construction techniques for hyperspectral image analysis," *IEEE Transactions on Geoscience and Remote Sensing*, vol. 55, no. 10, pp. 5966–5983, 2017.

[17] D. L. Donoho, "De-noising by soft-thresholding," *IEEE Transactions on Information Theory*, vol. 41, no. 3, pp. 613–627, 1995.

[18] D. C. Heinz and C.-I Chang, "Fully constrained least squares linear spectral mixture analysis method for material quantification in hyperspectral imagery," *IEEE Transactions on Geoscience and Remote Sensing*, vol. 39, no. 3, pp. 529–545, 2001.

[19] J. Chen, C. Richard, and P. Honeine, "Nonlinear unmixing of hyperspectral data based on a linear-mixture/nonlinear-fluctuation model," *IEEE Transactions on Signal Processing*, vol. 61, no. 2, pp. 480–492, 2013.

ISBN 978-90-827970-1-5 © EURASIP 2018